

Dark Matter microphysics and 21 cm observations

Laura Lopez-Honorez,^{1,2,*} Olga Mena,^{3,†} and Pablo Villanueva-Domingo^{3,‡}

¹*Service de Physique Théorique, CP225, Université Libre de Bruxelles, Bld du Triomphe, 1050 Brussels, Belgium*

²*Vrije Universiteit Brussel and The International Solvay Institutes, Pleinlaan 2, 1050 Brussels, Belgium.*

³*Instituto de Física Corpuscular (IFIC), CSIC-Universitat de Valencia, Apartado de Correos 22085, E-46071, Spain*

Dark matter interactions with massless or very light Standard Model particles, as photons or neutrinos, may lead to a suppression of the matter power spectrum at small scales and of the number of low mass haloes. Bounds on the dark matter scattering cross section with light degrees of freedom in such interacting dark matter (IDM) scenarios have been obtained from e.g. early time cosmic microwave background physics and large scale structure observations. Here we scrutinize dark matter microphysics in light of the claimed 21 cm EDGES 78 MHz absorption signal. IDM is expected to delay the 21 cm absorption features due to collisional damping effects. We identify the astrophysical conditions under which the existing constraints on the dark matter scattering cross section could be largely improved due to the IDM imprint on the 21 cm signal, providing also an explicit comparison to the WDM scenario.

I. INTRODUCTION

Interacting Dark Matter (IDM) with standard model light or massless degrees of freedom, such as photons and neutrinos, gives rise to a suppression of the small-scale matter power spectrum [1–4] (see also Refs. [5–10] for interactions with new (dark) light degrees of freedom). This damping is similar to the one caused by the free streaming of warm dark matter (WDM). In IDM scenarios, in contrast, the suppression of the small-scale overdensities is due to collisional damping [11–13]. These two alternatives to the standard Λ CDM model fall into the category of *non-cold dark matter* scenarios [14] (NCDM). Such dark matter models can provide some solutions to the the Λ CDM (where dark matter is made of purely cold and collisionless dark matter particles) *small scale crisis* (see e.g. the review of Ref. [15]). A large number of studies in the literature have been devoted to constrain the NCDM picture by means of cosmological probes, such as Cosmic Microwave Background (CMB) fluctuations and spectral distortions, galaxy clustering and Lyman- α forest power spectrum, the number of Milky Way satellites, the reionization history, or gravitational lensing [1–4, 13, 14, 16–58].

In this regard, the 21 cm signal offers a new cosmological probe, complementary to the existing ones, that could open a new window on the early universe and can further test the imprint of NCDM (see e.g. [59, 60] for early work on the subject). Here we will focus on the cosmic dawn period and in particular on the first claimed detection of an absorption feature in the sky-averaged global 21 cm signal at a redshift $z \sim 17$ by the experiment to Detect the Global Epoch of Reionization Signatures (EDGES) [61]. The measured amplitude of the dip in

the 21 cm global signal appears to be much deeper than that expected in standard CDM scenarios and therefore requires new physics to heat the radio background or cool the gas temperature, see also [62, 63] for other possible interpretations. This has triggered a surge of interest from the dark matter community trying to relate this effect to dark matter decay and annihilation [64–67]¹, and investigating the dark matter scenarios that could account for the signal, see e.g. [71–76].

While NCDM scenarios are unlikely to explain the large absorption amplitude, they delay structure formation and, therefore, might delay the onset of reionization and of UV and X-ray emission, see e.g. [43, 44, 58, 59]. As a result a shift to later times in the typical features in the 21 cm sky-averaged global signal and power spectrum is observed in the context of non-cold dark matter [58, 59, 77–79]. Consequently, it is timely to study the compatibility between the observation reported by EDGES, located at a redshift around $z \simeq 17$ and the IDM scenario. We follow two possible avenues. The first of them relies on exploiting the non-negligible Lyman- α coupling between the gas and the spin temperature characterizing the 21 cm signal at $z \simeq 20$ [78, 79]. The second one consists in imposing the minimum in the absorption feature to happen before $z \simeq 17$ [77]. For both strategies, a number of degeneracies between the details of dark matter microphysics and the astrophysical parameters will appear. We will briefly discuss their impact on the constraints on NCDM scenarios.

Universal fits to the halo mass functions from N-body simulations for the IDM scenarios have been obtained in [3, 80, 81]. In particular, here we will use the results of [80] derived for IDM scenarios involving dark matter-photon scatterings. A possible particle physics model related to this cosmological scenario is the case of millicharged dark matter [82, 83]. IDM scenarios including

* llopezho@ulb.ac.be

† olga.mena@ific.uv.es

‡ pablo.villanueva@ific.uv.es

¹ See also the previous works of Refs. [68–70].

dark matter-neutrino scatterings have been shown to give rise to a very similar damping in the power spectrum and also to a very similar mass function as for dark matter-photon scatterings, see Refs. [3, 12] and the Appendix A. Unfortunately, in the latter case, no publicly available dedicated analysis provides the necessary fits to the associated halo mass functions necessary for our study. We therefore use the IDM scattering on photons as a toy model to evaluate the impact of the EDGES signal on the more general case of IDM with light degrees of freedom. In order to ease comparison with previous studies, we shall also study the case of thermal warm dark matter (WDM) with mass in the keV range (see Refs. [33, 34, 42–57, 84–102] and the most recent works of Refs. [77, 79]).

The structure of the paper is as follows. We start in Sec. II by describing the physics of the 21 cm global signature. We account for the effect of IDM in the 21 cm

global signature in Sec. III, presenting the constraints on the dark matter photon elastic cross sections arising from (i) the presence of a rich Lyman- α background at $z \simeq 20$ (see Sec. III.1), and (ii) the location of the EDGES minimum (see Sec. III.2). Finally, we summarize our results and conclude in Sec. IV.

II. THE 21 CM SIGNAL

II.1. The differential brightness temperature

The brightness of a patch of neutral hydrogen (HI) relative to the CMB at a given redshift z is expressed in terms of the differential brightness temperature, δT_b . The sky-averaged δT_b scales as [103–106]

$$\frac{\delta T_b(\nu)}{\text{mK}} \simeq 27 x_{\text{HI}} \left(1 - \frac{T_{\text{CMB}}}{T_S} \right) \left(\frac{1+z}{10} \right)^{1/2} \left(\frac{0.15}{\Omega_m h^2} \right)^{1/2} \left(\frac{\Omega_b h^2}{0.023} \right), \quad (2.1)$$

where $\nu = \nu_{21}/(1+z)$ with $\nu_{21} = 1420$ MHz, x_{HI} represents the fraction of neutral hydrogen and $\Omega_b h^2$ and $\Omega_m h^2$ refer to the current baryon and matter contributions to the universe’s mass-energy content. The ratio of the populations of the two ground state hyperfine levels of hydrogen is quantified by the spin temperature, T_S , which is determined by three competing effects [107]: 1) absorption and stimulated emission of CMB photons coupling the spin temperature to the CMB temperature T_{CMB} in contrast with 2) atomic collisions (which are important at high redshifts $z \gtrsim 30$); and 3) resonant scattering of Lyman- α photons that couple the spin temperature to the gas kinetic temperature T_k . The latter effect is the so-called Wouthuysen-Field effect [108, 109] that turns on with the first sources. Assuming that the Lyman- α color temperature is $T_\alpha \simeq T_k$ [105], the spin temperature results from:

$$\left(1 - \frac{T_{\text{CMB}}}{T_S} \right) = \frac{x_{\text{tot}}}{1 + x_{\text{tot}}} \left(1 - \frac{T_{\text{CMB}}}{T_k} \right) \quad (2.2)$$

with $x_{\text{tot}} = x_\alpha + x_c$ and x_c and x_α are the coupling coefficients for collisions and Lyman- α scatterings.

At the low redshifts of interest here, collision coupling effects can be safely neglected and therefore, $x_{\text{tot}} = x_\alpha$. The Lyman- α coupling is defined as

$$x_\alpha = \frac{16\pi^2 T_\star e^2 f_\alpha}{27 A_{10} T_\gamma m_e c} S_\alpha J_\alpha, \quad (2.3)$$

where $T_\star = h\nu_{21} = 68.2$ mK is the hyperfine energy splitting, e and m_e the charge and mass of the electron, f_α is the oscillator strength of the Lyman- α transition, A_{10} is the spontaneous decay rate of the 21 cm transition,

J_α is the specific intensity of the background radiation evaluated at the Lyman- α frequency and S_α is an order unity correction factor which accounts for the detailed shape of the spectrum near the resonance [110]. In particular, in the framework considered here, $S_\alpha \lesssim 1$ and the Lyman- α flux gets two types of contributions. One results from the X-ray excitation of HI ($J_{\alpha X}$), while the other one results from direct stellar emission of UV photons between Lyman- α and the Lyman- α limit $J_{\alpha\star}$, thus $J_\alpha = J_{\alpha X} + J_{\alpha\star}$ [111]. We will see in Sec. II.2 that for the X-ray efficiencies considered here, $J_{\alpha X}$ only represents a small contribution to the total Ly α flux. On the other hand, the direct stellar emission contribution to J_α is computed assuming by default a Pop II stars spectral model. This gives rise to the emission of 9690 photons per baryon between Lyman- α and the Lyman limit, see Appendix B (see also [112]). Notice from Eq. (2.2) that, when $x_{\text{tot}} = x_\alpha = 1$, δT_b will be at the half of the value that it would have if T_S were completely coupled to T_k , which happens when $x_\alpha \gg 1$. The authors of Ref. [79], following the EDGES results [61], have imposed that x_α should be one or larger at redshift $z \simeq 20$. We shall apply this constraint in our numerical analyses of IDM scenarios, see Sec. III.1.

In order to extract the imprint of NCDM on the 21 cm signal, we profit from the publicly available tool **21cmFast**. The main purpose of the code is the study of variations in the 21 cm signal due to changes in a given set of astrophysical and cosmological parameters. We make use of the output values of x_α and of T_S and x_{HI} to extract the differential brightness temperature as in Eq. (2.1). In practice, we use a version of the **21cmFast** code adapted to account for the IDM and the WDM as

detailed in Ref. [58]. We have modified the default WDM scenario implementation modifying the definition of both the transfer function and the halo mass function according to the prescription given in the Appendix A. This halo mass function plays an important role in the evaluation of the production rate of ultraviolet (UV), X-rays, and Lyman- α radiation, responsible of the ionization, heating and Lyman- α coupling respectively. These production rates are proportional to the star formation rate $\dot{\rho}_*$. In 21cmFast, this quantity is evaluated in terms of the growth of the fraction of mass collapsed in haloes which are able to host star-forming galaxies, $f_{\text{coll}}(> M_{\text{vir}}^{\text{min}})$, defined as

$$f_{\text{coll}}(> M_{\text{vir}}^{\text{min}}) = \frac{1}{\rho_{m,0}} \int_{M_{\text{vir}}^{\text{min}}}^{\infty} M \frac{dn}{dM} dM, \quad (2.4)$$

where $\rho_{m,0}$ is the current matter density and dn/dM is the halo mass function. For the NCDM cosmologies, the halo mass function is always suppressed at small masses compared to the CDM scenario, giving rise to a smaller f_{coll} , at fixed redshift, as illustrated in Fig. 1, see also [1, 59, 113].² With the purple area we show the case of CDM with threshold masses $M_{\text{vir}}^{\text{min}}$ between $10^6 M_{\odot}$ (upper curve) and $3 \times 10^7 M_{\odot}$ (lower curve) at $z = 20$ or equivalently $T_{\text{vir}}^{\text{min}}$ between 10^3 and 10^4 K, see eq. (2.5). The upper purple curve for CDM can be compared to case of NCDM scenarios in the form of WDM (red, blue and cyan continuous curves) and of IDM (red, blue and cyan dotted curves) for the same $M_{\text{vir}}^{\text{min}} = 10^6 M_{\odot}$ at $z = 20$ ($T_{\text{vir}}^{\text{min}} = 10^3$ K). The IDM scattering cross-sections are normalized in terms of the Thompson cross section $\sigma_T = 6.65 \times 10^{-25} \text{ cm}^2$.

Overall, in the framework considered here, the NCDM modification of f_{coll} will result into a delayed reionization, heating and Lyman- α coupling, giving rise to an absorption feature in the 21 cm signal located at lower redshifts with respect to CDM scenarios [43, 44, 58, 59]. Notice also that curves of a fixed color in Fig. 1 correspond to IDM and WDM models giving rise to a fixed value of the half-mode mass or breaking scale of the linear power spectrum, see Eqs. (A6), (A7) and (A9) in Appendix A. For fixed half-mode mass, the suppression of the f_{coll} is always more severe in the WDM scenarios than in the IDM scenarios due to a relatively larger number of low mass haloes in the IDM case, see [80]. The rate at which f_{coll} increases with redshift is also different between IDM and WDM. These features might help to discriminate between NCDM models using both the 21 cm global signal and its power spectrum [58].

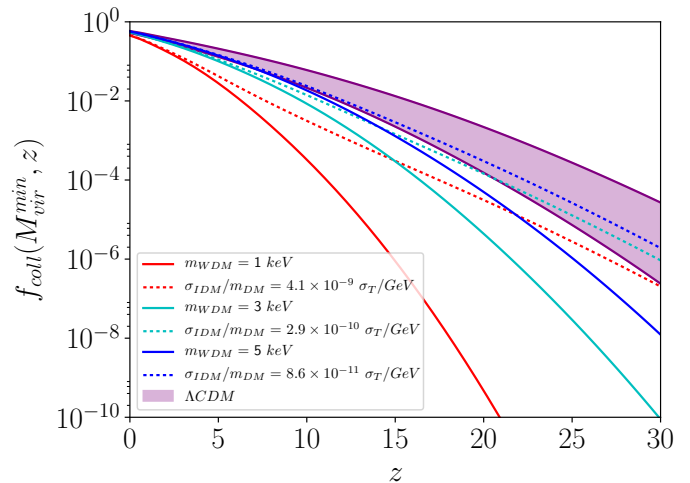


FIG. 1. Fraction of mass collapsed into haloes of mass larger than $M_{\text{vir}}^{\text{min}}(z = 20) \simeq 10^6 M_{\odot}$ (corresponding to $T_{\text{vir}}^{\text{min}} = 10^3$ K) as a function of the redshift. The continuous lines depict the WDM cases that are compared with IDM scenarios, shown with dotted curves. Continuous and dotted curves of the same colors corresponds to a fixed value of the half-mode mass. The purple region illustrates the change in the CDM collapsed fraction (using the Sheth-Tormen mass function) for $T_{\text{vir}}^{\text{min}}$ varying within the range of 10^3 to 10^4 K.

II.2. The astrophysical parameters

The minimum virial mass $M_{\text{vir}}^{\text{min}}$ from which haloes begin to efficiently form stars (see Eq. (2.4)) is related to the threshold temperature $T_{\text{vir}}^{\text{min}}$ as [115]

$$M_{\text{vir}}^{\text{min}}(z) = 10^8 \left(\frac{T_{\text{vir}}^{\text{min}}}{1.98 \times 10^4 \text{ K}} \frac{0.6}{\mu} \right)^{3/2} \left(\frac{1+z}{10} \right)^{-3/2} M_{\odot}/h, \quad (2.5)$$

where μ is the mean molecular weight and it is equal to 1.2 (0.6) for a neutral (fully ionized) primordial gas. The value of the minimum virial temperature depends on the cooling mechanism considered. The lower threshold to make the atomic cooling channel effective is $T_{\text{vir}}^{\text{min}} = 10^4$ K [116–120], corresponding to $M_{\text{vir}}^{\text{min}} = 3 \times 10^7 M_{\odot}$ at $z = 20$ for $\mu = 0.6$. In contrast, the molecular H_2 cooling channel can be effective down to temperatures of $T_{\text{vir}}^{\text{min}} = 10^3$ K corresponding to $M_{\text{vir}}^{\text{min}} = 10^6 M_{\odot}$ at $z = 20$. The hydrogen molecules may however be destroyed by the ionizing radiation. Nevertheless, several hydrodynamical works in the literature [121, 122] have shown that in the presence of a large soft UV background, molecular cooling could be highly effective, i.e. metal-enriched star formation is not restricted to atomic cooling. Furthermore, even in the absence of electrons, molecular cooling could cool down the gas in haloes associated to virial temperatures much lower than the ones required for atomic cooling. Consequently, in the following, we shall consider $T_{\text{vir}}^{\text{min}} = 10^3$ K as the minimum threshold temperature for star formation and we assume the same threshold temperature $T_{\text{vir}}^{\text{min}}$ for haloes host-

² Let us emphasize that our prescription for WDM differs from one of [59]. Here we follow the fits to the results of simulations from [90] for WDM which was directly compared to the results of IDM simulations in [3, 81, 114]. Reference [59] followed an earlier prescription introduced by [45].

ing ionizing and X-ray sources. This parameter plays a crucial role in extracting the constraints from the 21 cm absorption signal in both CDM and NCDM scenarios, see also [77, 78]. The impact of varying $T_{\text{vir}}^{\text{min}}$ in the 10^3 K to 10^4 K range within the CDM paradigm is illustrated in Fig. 1 with the purple area. The lower value of the threshold parameter corresponds to higher values of the fraction of collapsed haloes at a given redshift.

The comoving star formation rate density is described by $\dot{\rho}_* = f_* \rho_{b,0} f_{\text{coll}}(> M_{\text{vir}}^{\text{min}})$, where f_* , the fraction of baryons that are converted into stars, considered here as a constant parameter (neglecting any dependence on the halo masses or redshift). As f_* controls the amplitude of the star formation rate density, it also sets the amplitude of both the ionizing and heating rates, as well as the Lyman- α flux. This parameter is quite uncertain as no observations of low mass mass haloes of mass $10^6 - 10^8 M_\odot$ at redshift $z \sim 20$ are available. Nevertheless, several previous works, based on radiation-hydrodynamic simulations of high-redshift galaxies in a neutral medium [122–125] or based on the comparison of the star formation rate density to the one derived from UV luminosity function measurements [79, 126, 127], have found values of $f_* \sim \mathcal{O}(0.01)$. In the following, we therefore consider $f_* = 0.01$, leaving for the discussion in Sec. IV the impact in our results of slightly larger values of f_* .

Finally, in order to characterize the overall normalization of the X-ray luminosity, 21cmFast makes use of the X-ray efficiency parameter ζ_X , expressed in units of M_\odot^{-1} . This parameter is varied here within the range $\zeta_X = [1 - 5] \times 10^{56}/M_\odot$. One can relate this parameter to the integrated X-ray soft band emissivity (below 2 keV) per unit of star formation rate escaping the galaxy $L_{X<2\text{keV}}/\text{SFR}$, varied in the range $\log_{10}(L_{X<2\text{keV}}/\text{SFR}) \in [39.5, 40.2]$ erg/s / (M_\odot/yr).³ This range is similar to one extracted from observations of the hot interstellar medium, which lead to $\log_{10}(L_{X<2\text{keV}}/\text{SFR}) \sim [39, 40]$ erg/s / (M_\odot/yr) [129], and also to the one adopted in Ref. [77] (see also Ref. [130]).

III. IMPRINT OF THE IDM ON THE 21 CM SIGNAL

Non-cold dark matter scenarios are expected to delay structure formation and therefore the absorption feature in the 21 cm signal at cosmic dawn. This effect is illustrated for the IDM model under study in Fig. 2,

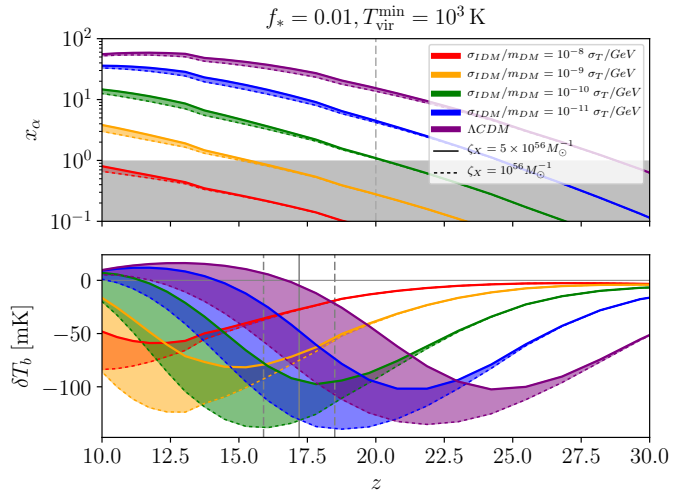


FIG. 2. Coupling coefficient for Lyman- α scattering (top) and sky-averaged 21 cm brightness temperature (bottom) as a function of the redshift for several possible values of the scattering dark matter-photon cross-section over the dark matter particle mass. We have fixed $f_* = 0.01$ and $T_{\text{vir}}^{\text{min}} = 10^3$ K. The width of the bands refers to the change in δT_b and x_α due to different values of ζ_X .

where we show the coupling coefficient for Lyman- α scattering x_α (top), and the sky-averaged 21 cm brightness temperature (bottom). The different colors correspond to different values of the dark matter-photon scattering cross-sections over the dark matter particle mass, $\sigma_{\text{IDM}}/\sigma_T(\text{GeV}/m_{\text{DM}})$. As can be noticed, large cross sections, inducing a stronger suppression at small scales, also induce a stronger suppression of the Lyman- α coupling at a given redshift (see the top panel of Fig. 2) and a larger shift towards smaller redshifts of the 21 cm features (see the bottom panel of Fig. 2). We also illustrate, with a vertical line, the position of the minimum of absorption reported by the EDGES experiment (at $\nu = 78$ MHz corresponding to $z = 17.2$). The dashed lines correspond to the largest signal redshift range at the minimum of absorption within the 99% CL interval reported by Ref. [61].

Figure 2 also shows the impact of varying the X-ray heating efficiency ζ_X in the $10^{56} M_\odot^{-1} - 5 \times 10^{56} M_\odot^{-1}$ range with the width of the colored bands. We see from the top panel of Fig. 2 that the range of ζ_X considered here, the Lyman- α flux resulting from X-ray excitation ($J_{\alpha X} \propto \zeta_X$) is usually a negligible contribution to the Lyman- α coupling at the redshift at which $x_\alpha \sim 1$. On the bottom panel of Fig. 2, we see the impact of the X-ray heating parameter ζ_X on the differential brightness temperature. Here the impact is more significant. The deepest absorption dip corresponds to $\zeta_X = 10^{56} M_\odot^{-1}$, while the shallowest one is obtained for $\zeta_X = 5 \times 10^{56} M_\odot^{-1}$. Notice also that a larger value of ζ_X implies an earlier minimum, i.e. the X-ray heating of the IGM occurs earlier in time. As a result, in order to extract conservative

³ The emissivity $L_{X<2\text{keV}}/\text{SFR}$ corresponds to the following combination of parameters: $\alpha_X \zeta_X h_p \int (\nu/\nu_0)^{-\alpha_X} d\nu$ where h_p is the Planck constant, α_X is the spectral slope parameter and ν_0 is the obscuration frequency cutoff parameter (see the 21cMMC code [128] based on 21cmFast). The integral goes from ν_0 to 2 keV. We took $\alpha_X = 1.2$ and $\nu_0 = 7.2 \times 10^{12}$ Hz (corresponding to an energy of 300 eV), that are the default values in the 21cmFast code.

constraints on the NCDM parameters from the redshift at which the absorption minimum is located, we shall consider the value $\zeta_X = 5 \times 10^{56}/M_\odot$, see Sec. III.2.

Figure 3 illustrates the equivalent to Fig. 2 with ζ_X fixed to $5 \times 10^{56} M_\odot^{-1}$ and considering this time $T_{\text{vir}}^{\text{min}} = 10^3$ K (continuous curves) as well as $T_{\text{vir}}^{\text{min}} = 10^4$ K (dotted curves). Going from left to right panel of Fig. 3 we increase the value of f_* by a factor of 3. Based on these plots, we discuss in the next two subsections the constraints that could be derived on NCDM scenarios following two different approaches.

III.1. Constraints from the Lyman- α background

In order to account for the EDGES results, the authors of Ref. [79] based their analyses on the assumption that a sufficiently strong Lyman- α background is present by $z \sim 20$. They imposed

$$x_\alpha(z=20) \gtrsim 1. \quad (3.1)$$

This limit results from the observation that the absorption signal reported by the EDGES experiment is equal to half of the maximum amplitude of absorption at $z \simeq 20$. We shall follow this assumption here, applying this condition to our simulations within NCDM models. Let us first focus on the top left panel of Fig. 3, which shows the Lyman- α coupling coefficient x_α as a function of the redshift for $f_* = 0.01$. The condition reported in (3.1) disfavors the cosmological scenarios associated to a prediction of $x_\alpha(z)$ lying within the shaded area at $z = 20$.

The astrophysical parameter $T_{\text{vir}}^{\text{min}}$ has a significant impact on the Lyman- α coupling coefficient x_α . Larger virial temperature shifts star formation to lower redshifts, giving rise to a lower Lyman- α background at a given redshift. In a similar way, a large value of the IDM scattering cross-section implies a longer delay in structure formation. As a result, one can deduce from Fig. 3 (left panel) that, for molecular cooling ($T_{\text{vir}}^{\text{min}} = 10^3$ K), the scattering cross-section must be below $10^{-10} \sigma_T \times (m_{\text{DM}}/\text{GeV})$. If one assumes instead that the only efficient cooling mechanism is atomic cooling with $T_{\text{vir}}^{\text{min}} \geq 10^4$ K, the limits on the IDM scattering cross section become much tighter, excluding scattering cross-section lower than $10^{-11} \sigma_T \times (m_{\text{DM}}/\text{GeV})$. Our most conservative bound (assuming $f_* = 0.01$) is therefore $\sigma_{\text{IDM}} \lesssim 10^{-10} \sigma_T \times (m_{\text{DM}}/\text{GeV})$. This constraint is stronger than the 95% CL upper limit of $\sigma_{\text{IDM}} < 8 \times 10^{-10} \sigma_T \times (m_{\text{DM}}/\text{GeV})$ reported in Ref. [58], based on observations of Milky Way satellite galaxy number counts and assuming a mass for our galaxy of $M_{\text{MW}} = 2.6 \times 10^{12} M_\odot$.

Notice that the Lyman- α coupling coefficient x_α is directly proportional to the fraction of baryons converted into stars (f_*), here considered as constant. The left (right) panels of Fig. 3 have been simulated with $f_* = 0.01$ ($f_* = 0.03$). Notice that larger values of f_* increase the Lyman- α coupling at a fixed redshift,

weakening the bound on IDM scenarios resulting from Eq. (3.1). In the case of $f_* = 0.03$, the limits quoted above are translated into $\sigma_{\text{IDM}} \lesssim 10^{-9} \sigma_T \times (m_{\text{DM}}/\text{GeV})$ and $\sigma_{\text{IDM}} \lesssim 10^{-10} \sigma_T \times (m_{\text{DM}}/\text{GeV})$ for $T_{\text{vir}}^{\text{min}} = 10^3$ K and $T_{\text{vir}}^{\text{min}} = 10^4$ K respectively.

III.2. Constraints from the position of the absorption minimum in the 21 cm global signature

Another possible avenue to constrain NCDM models using the EDGES observations is based on the location of the minimum of the absorption. Reference [77] imposed that it should be located at a redshift higher than $z = 17.2$ and studied the resulting bounds on a large set of NCDM models. We show in the bottom panels of Fig. 3 the effect of the IDM scenario considered here on the global sky-averaged 21 cm brightness temperature obtained by means of Eq. (2.1).

Let us focus first in the $f_* = 0.01$ case (i.e. left panel). Considering atomic cooling (dotted curves with $T_{\text{vir}}^{\text{min}} = 10^4$ K), it appears that for scattering cross sections larger than $\sim 10^{-11} \sigma_T \times (m_{\text{DM}}/\text{GeV})$ the absorption minimum takes place at redshifts lower than $z = 17.2$. Such cross-sections should therefore be regarded as disfavored. Considering molecular cooling softens this constraint by \sim one order of magnitude (see the continuous curves for $T_{\text{vir}}^{\text{min}} = 10^3$ K). Notice that we have considered a conservative X-ray efficiency of $\zeta_X = 5 \times 10^{56} M_\odot^{-1}$ for all curves. Considering lower values of ζ_X will give rise to a later X-ray heating and thus a minimum of absorption located at lower redshifts.

If instead, we consider a larger fraction of baryons converted into stars, $f_* = 0.03$, (see the bottom right panel), and $T_{\text{vir}}^{\text{min}} = 10^3$ (10^4) K, the limit on the IDM interactions is relaxed, excluding cross sections above $\sim 10^{-9}$ (10^{-10}) $\sigma_T \times (m_{\text{DM}}/\text{GeV})$. This is due to the fact that both the X-ray and the Lyman- α emission rates are directly proportional to f_* . Increasing f_* implies an earlier Lyman- α coupling and X-ray heating periods, displacing the minimum of the absorption in the 21cm signal to a larger redshift.

IV. DISCUSSION AND CONCLUSIONS

Interacting Dark Matter (IDM) models, in which dark matter is not made out of purely cold, pressureless particles, are an interesting alternative to the standard CDM paradigm and provide a possible avenue to alleviate the so-called small-scale crisis of the Λ CDM. The IDM could be scattering off light or massless degrees of freedom such as photons or neutrinos. Here we have considered the case of dark matter scattering on photons, characterized by the size of the scattering rate over the DM mass, $\sigma_{\text{IDM}}/m_{\text{DM}}$. The reason for this choice is driven by the availability of a fitting function for the halo mass function relevant for our study. Let us emphasize though

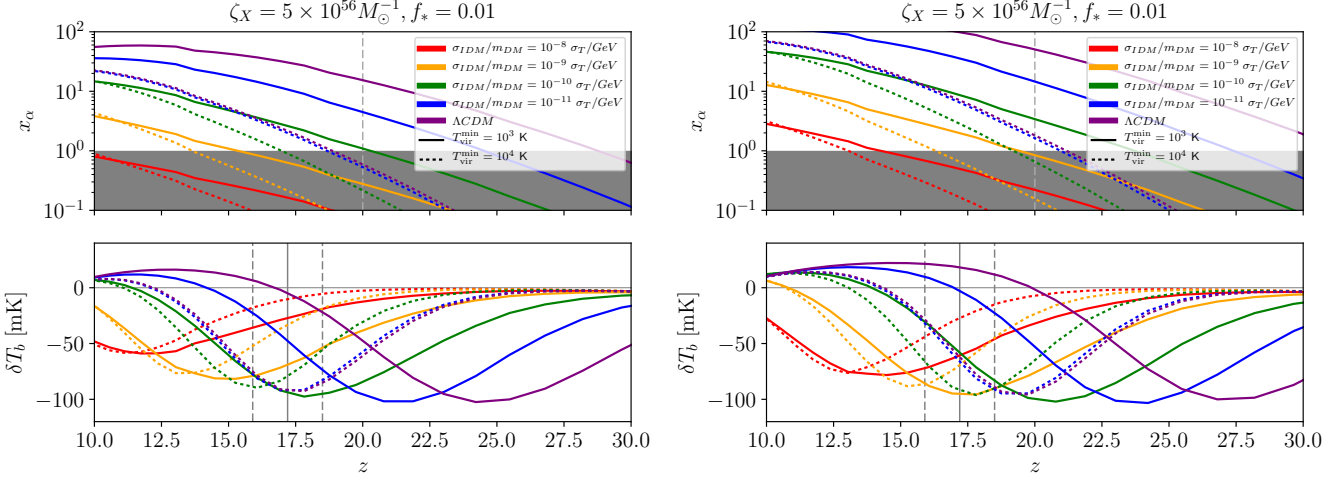


FIG. 3. Top panels: Lyman- α coupling coefficient x_α versus redshift for different values of the astrophysical parameter $T_{\text{vir}}^{\text{min}}$ and for several possible values of the scattering dark matter-photon cross-section over the dark matter mass. Cases within the shaded region are highly disfavoured by the condition given by Eq. (3.1). Bottom panels: sky-averaged 21 cm brightness temperature. The solid (dashed) lines indicate the mean redshift (range in redshift) associated to the EDGES signal. We have fixed $\zeta_X = 5 \times 10^{56} M_\odot^{-1}$ and $f_* = 0.01$ ($f_* = 0.03$) in left (right) panel.

that scatterings on neutrinos are expected to give rise to a similar imprint on the 21 cm signal.

Several studies have constrained IDM models based on their suppression of clustering at small scales, exploiting galaxy power spectrum, gravitational lensing, CMB, number of Milky Way dwarf galaxies and Lyman- α forest observations, among others. Here we focus on the imprint of IDM on the 21 cm signal arising from cosmic dawn. Based on a modified version of the **21cmFast** code, our simulations show that IDM delays the formation of haloes capable of star formation, shifting the timing of the 21 cm signal features compared to the standard CDM scenario. A similar effect has been reported in the case of other NCDM models [43, 44, 58, 59]. In this paper, we have considered two possible ways to test the IDM properties against the 21 cm signal. First, following Ref. [79], a significant Lyman- α coupling between the gas and the spin temperature characterizing the 21 cm signal should be present at $z = 20$. Secondly, as argued in Ref. [77], the location of the absorption minimum in the EDGES signal at $z = 17.2$ implies that any scenario with sufficiently enough delayed structure formation could be discarded.

We have first identified which are the most relevant astrophysical parameters showing large degeneracies with the IDM scattering cross-section over the mass $\sigma_{\text{IDM}}/m_{\text{DM}}$. Namely, the fraction of baryons into stars f_* , the threshold temperature for haloes to host star-forming galaxies $T_{\text{vir}}^{\text{min}}$ and the X-ray efficiency, ζ_X , have been shown to interfere with the eventual extraction of a non-zero σ_{IDM} . Fortunately, the parameter ζ_X only plays a significant role in extracting the location of the absorption minimum, and we have adopted the conservative value of $\zeta_X = 5 \times 10^{56} M_\odot^{-1}$ (corresponding to an integrated soft band X-ray emissivity of $L_{X < 2\text{keV}}/\text{SFR} =$

$10^{40.2} \text{ erg/s} / (M_\odot/\text{yr})$). We also considered a lower limit on the threshold virial temperature of $T_{\text{vir}}^{\text{min}} = 10^3 \text{ K}$ (corresponding to molecular cooling) as well as a constant value of $f_* < 0.03$.

Our results are summarized on the left panel of Fig. 4 in the case of $f_* = 0.01$. The top panels show the Lyman- α coupling coefficient x_α at $z = 20$ for $T_{\text{vir}}^{\text{min}} = 10^3$ (10^4) K with the top blue (bottom red) curve as a function of the IDM scattering cross-section. Notice that the $x_\alpha(z = 20)$ curves saturate to a maximum value at low enough values of the scattering cross-section. This corresponds to the limiting $x_\alpha(z = 20)$ value that one would get in the CDM scenario (indicated with the horizontal dotted lines). In addition, the shaded region refers to the parameter space in which the condition $x_\alpha(z = 20) > 1$ can not be satisfied and can therefore be considered as disfavoured by the condition given by Eq. (3.1). As a result, for $f_* = 0.01$ and $\zeta_X = 5 \times 10^{56} M_\odot^{-1}$, a value of $\sigma_{\text{IDM}} > 10^{-10} \sigma_T \times (m_{\text{DM}}/\text{GeV})$ fails to satisfy the condition $x_\alpha(z = 20) > 1$ when considering molecular cooling ($T_{\text{vir}}^{\text{min}} = 10^3 \text{ K}$). This improves the previous bound derived on such IDM model in Ref. [58]. When considering higher threshold temperatures for efficient cooling, the bounds get tighter, disfavoured even the canonical CDM scenario if $T_{\text{vir}}^{\text{min}} = 10^4 \text{ K}$. All these limits would be relaxed if the fraction of baryons converted into stars is larger, as it was illustrated in Fig. 3 for $f_* = 0.03$. For instance, for $T_{\text{vir}}^{\text{min}} = 10^3 \text{ K}$, the limit would be reduced by one order of magnitude (i.e. $\sigma_{\text{IDM}} < 10^{-9} \sigma_T \times (m_{\text{DM}}/\text{GeV})$).

In the bottom left panel of Fig. 4, we show the redshift at which the sky-averaged 21 cm brightness temperature exhibits its minimum of absorption at cosmic dawn, $z(\delta T_b^{\text{min}})$, as a function of the IDM scattering

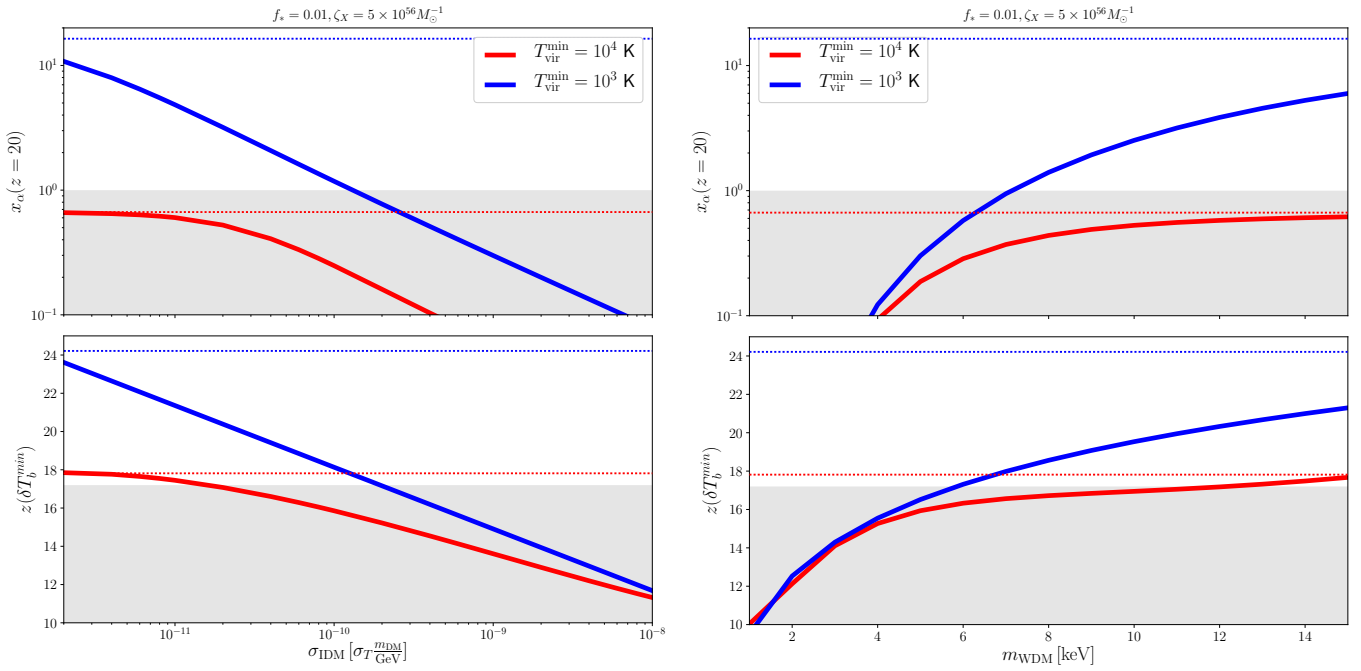


FIG. 4. Left, top (bottom) panel: Lyman- α coupling coefficient x_α at $z = 20$ (redshift of the absorption minimum in the sky-averaged 21 cm brightness temperature) versus the scattering dark matter-photon cross-section for $T_{\text{vir}}^{\text{min}} = 10^4$ K (atomic cooling) and for $T_{\text{vir}}^{\text{min}} = 10^3$ K (molecular cooling). Right panels: the same but for WDM models, as a function of the WDM mass m_{WDM} . IDM/WDM scenarios lying in the shaded regions are highly disfavoured by the two conditions exploited here, see text for details. We have fixed $f_* = 0.01$ and $\zeta_X = 5 \times 10^{56} M_\odot^{-1}$. Dashed lines stand for the results in the CDM scenario.

cross-section. Again $z(\delta T_b^{\text{min}})$ saturates for low enough scattering cross-section to a value corresponding to the the CDM limit denoted with a dotted horizontal line. The shaded area denotes the region in which this minimum is located below $z = 17.2$. More concretely, in order to derive the curves shown in the bottom panels of Fig. 4, we have fitted the brightness temperature curves obtained from our simulations to the flattened gaussian shape that the EDGES collaboration uses to model the 21 cm absorption profile [61]. This procedure allows us to extract the central frequency for each possible value of $\sigma_{\text{IDM}}/m_{\text{DM}}$, $T_{\text{vir}}^{\text{min}}$ and f_* , and also to constrain the model by imposing that this mean frequency ν_0 of our flattened gaussian fits should lie at frequencies below the lower 99% confidence interval (including estimates of systematic uncertainties) reported by the EDGES collaboration for the $\nu_0 = 78$ MHz parameter. From Fig. 4, the position of the minimum of absorption disfavours the region $\sigma_{\text{IDM}} > 10^{-10} \sigma_T \times (m_{\text{DM}}/\text{GeV})$ ($\sigma_{\text{IDM}} > 10^{-11} \sigma_T \times (m_{\text{DM}}/\text{GeV})$) for $T_{\text{vir}}^{\text{min}} = 10^3$ K ($T_{\text{vir}}^{\text{min}} = 10^4$ K). As in the case of the $x_\alpha(z = 20) > 1$ condition, these limits would be relaxed by one order of magnitude in the case of a value of $f_* = 0.03$. Also, for the astrophysical parameters considered here, we see that the constraints from the Lyman- α coupling condition are typically tighter than those arising from the position of the minimum of absorption.

Summarizing, for $f_* \simeq 0.01$, $\zeta_X < 5 \times 10^{56} M_\odot^{-1}$ and

$T_{\text{vir}}^{\text{min}} > 10^3$ K, the bounds on $\sigma_{\text{IDM}}/m_{\text{DM}}$ derived in this work imply an order of magnitude improvement over the most constraining existing limits in the literature [2, 58]. Larger values of f_* may compromise these upgraded limits. In order to ease the comparison to other studies on NCDM scenarios, we provide the results obtained following the same methodology in a thermal warm dark matter scenario involving light dark matter particles with a mass m_{WDM} of a few keV. The prescription considered here to describe the suppression of the halo mass function at small halo masses is given in the Appendix A. We show the obtained dependence of $x_\alpha(z = 20)$ and $z(\delta T_b^{\text{min}})$ in the right panel of Fig. 4. From this figure with $f_* = 0.01$ and $\zeta_X = 5 \times 10^{56} M_\odot^{-1}$, we can infer a lower limit in the WDM mass around $m_{\text{WDM}} > 6$ keV ($m_{\text{WDM}} > 12$ keV) if $T_{\text{vir}}^{\text{min}} = 10^3$ K ($T_{\text{vir}}^{\text{min}} = 10^4$ K). These tight limits are similar to those derived in Refs. [77, 79] for slightly different WDM implementations and astrophysical parameters.

Appendix A: Halo mass functions

The halo mass function, that counts the number of haloes per unit halo mass and volume at a given redshift, can be written as [131]

$$\frac{dn}{dM} = -\frac{1}{2} \frac{\rho_m}{M^2} f(\nu) \frac{d \ln \sigma^2}{d \ln M}, \quad (\text{A1})$$

where n is the halo number density, $\rho_m = \Omega_m \rho_c$ is the average matter density in the Universe at $z = 0$ and $\sigma^2 = \sigma^2(M, z)$ is the variance of density perturbations, which is a function of the halo mass M and redshift. The first-crossing distribution, $f(\nu)$, is expected to be a universal function of $\nu \equiv \delta_c^2 / \sigma^2(M, z)$, with $\delta_c = 1.686$, the linearly extrapolated density for collapse at $z = 0$. The Sheth-Tormen (ST) first-crossing distribution reads as [132–134]:

$$f(\nu) = A \sqrt{\frac{2q\nu}{\pi}} (1 + (q\nu)^{-p}) e^{-q\nu/2}, \quad (\text{A2})$$

with $p = 0.3$, $q = 0.707$ and $A = 0.3222$. For the standard CDM scenario, we consider this first-crossing distribution. The variance at $z = 0$, $\sigma(M) \equiv \sigma(M, z = 0)$, at a given scale R can be expressed as

$$\sigma_X^2(M(R)) = \int \frac{d^3k}{(2\pi)^3} P_X(k) W^2(kR), \quad (\text{A3})$$

where $P_X(k)$ is the linear power spectrum at $z = 0$ for a given $X = \{\text{CDM, IDM or WDM}\}$ cosmology and W is the Fourier transform of a filter function that we consider to be a top-hat (TH) function in real space (see e.g. [14, 77] for the possibility of using a sharp- k window function for NCDM). The redshift dependence is driven by the linear growth function, $D(z)$ normalized to 1 at $z = 0$, so that the root-mean-square (rms) density fluctuation is $\sigma(M, z) = \sigma(M, z = 0) D(z)$.

The transfer function T_X for a NCDM scenario X is defined as

$$P_X(k) = P_{\text{CDM}}(k) T_X^2(k), \quad (\text{A4})$$

where $P_{\text{CDM}}(k)$ is the linear power spectrum in Λ CDM. Here we use the prescription of Refs. [12, 84]:

$$T_X(k) = (1 + (\alpha_X k)^{2\mu})^{-5/\mu}, \quad (\text{A5})$$

where $\mu = 1.2$ is a dimensionless exponent and α_X is a breaking scale. The latter takes the form:

$$\alpha_{\text{WDM}} = 0.048 \left(\frac{\text{keV}}{m_{\text{WDM}}} \right)^{1.15} \left(\frac{\Omega_{\text{WDM}}}{0.4} \right)^{0.15} \left(\frac{h}{0.65} \right)^{1.3} \text{Mpc}/h, \quad (\text{A6})$$

$$\alpha_{\gamma\text{DM}} = 0.073 \left[10^8 \left(\frac{\sigma_{\text{IDM}}}{\sigma_T} \right) \left(\frac{\text{GeV}}{m_{\text{DM}}} \right) \right]^{0.48} \left(\frac{\Omega_{\text{WDM}}}{0.4} \right)^{0.15} \left(\frac{h}{0.65} \right)^{1.3} \text{Mpc}/h. \quad (\text{A7})$$

for WDM scenarios [3, 90] and IDM involving dark matter-photon scattering [12] respectively. For DM-neutrino interactions, described with the same parametrization of the transfer function, one gets a breaking scale $\alpha_{\nu\text{DM}} \simeq 0.8 \times \alpha_{\gamma\text{DM}}$ for a fixed value of the scattering cross section [3].

The halo mass function defined as in Eq. (A1) is well suited for CDM but it needs to be adapted for the NCDM case. In order to match the results from N-body simulations, the WDM halo mass function can be expressed as [90]

$$\frac{dn^{\text{WDM}}}{dM} = \left(1 + \frac{M_{\text{hm}}}{bM} \right)^a \frac{dn^{\text{ST, WDM}}}{dM}, \quad (\text{A8})$$

where an additional mass-dependent correction to the standard ST formalism appears. We use $a = -0.6$ and $b = 0.5$, as obtained in [3, 80]. The function $\frac{dn^{\text{ST, WDM}}}{dM}$ in Eq. (A8) refers to the halo mass function obtained with a ST first-crossing distribution, as defined in Eq. (A2), and a linear matter power spectrum corresponding to the WDM case. In order to describe the suppression in the linear regime, one can consider the half-mode mass M_{hm} , defined as the mass scale for which $T_X/T_{\text{CDM}} = 1/2$ (i.e. $P_X/P_{\text{CDM}} = 1/4$). Using the general fit to the transfer function, Eq. (A5), the half-mode mass M_{hm} can be

easily derived as

$$M_{\text{hm}} \equiv \frac{4\pi}{3} \rho_m (\pi\alpha_X)^3 (2^{\mu/5} - 1)^{-3/(2\mu)}. \quad (\text{A9})$$

For what concerns the IDM models, the number of low-mass structures appears to be larger than in WDM scenarios [3] (see also [7]). In order to reproduce the IDM results for masses below the half-mode mass, an extra mass-dependent correction must be introduced to the halo mass function [80]:

$$\frac{dn^{\text{IDM}}}{dM} = \left(1 + \frac{M_{\text{hm}}}{bM} \right)^a \left(1 + \frac{M_{\text{hm}}}{gM} \right)^c \frac{dn^{\text{ST, CDM}}}{dM}, \quad (\text{A10})$$

with $a = -1$, $b = 0.33$, $g = 1$, $c = 0.6$ and $\frac{dn^{\text{ST, CDM}}}{dM}$ refers to the standard ST first-crossing distribution as defined in Eq. (A2) with the CDM linear power spectrum for the variance of density perturbations.

Appendix B: Lyman- α emissivity

The Lyman- α flux from direct stellar emission of UV photons, $J_{\alpha*}$, is given by the sum over the Lyman- n levels which can lead to a $2p \rightarrow 1s$ transition through a decaying cascade. Due to the optical thickness of the IGM, photons which redshift to a Lyman resonance are

absorbed by the medium. A photon which reaches a Lyman- n resonance at redshift z has to be emitted at a redshift below $1 + z_{max,n} = \frac{1-(n+1)^{-2}}{1-n^{-2}}(1+z)$. If $f_{rec}(n)$ is the recycled fraction of the level n , *i.e.*, the probability of generating a Lyman- α photon from the n level [135], the total Lyman- α flux can be written as

$$J_{\alpha\star} = \frac{c(1+z)^2}{4\pi} \sum_{n=2}^{n_{max}} f_{rec}(n) \int_z^{z_{max,n}} dz' \frac{\epsilon_{\alpha}(\nu'_n, z')}{H(z')}, \quad (\text{B1})$$

where the emission frequency is $\nu'_n = \nu_n \frac{1+z'}{1+z}$, being $\nu_n = \nu_{LL}(1 - n^{-2})$ and ν_{LL} the Lyman limit frequency. The comoving emissivity ϵ_{α} can be written as proportional to the star formation rate $\dot{\rho}_{\star}$:

$$\epsilon_{\alpha}(\nu, z) = \varepsilon(\nu) \frac{\dot{\rho}_{\star}(z)}{\mu m_p} = \varepsilon(\nu) f_{\star} \bar{n}_{b,0} \dot{f}_{coll}(z), \quad (\text{B2})$$

where $\bar{n}_{b,0}$ is the comoving number density of baryons. Assuming that only Population-II stars contribute to this emissivity, the spectral distribution $\varepsilon(\nu)$ is given by a separate power law between each Lyman- n and Lyman- $n+1$ levels:

$$\varepsilon(\nu) = N_n \frac{(\beta_n + 1) \nu_{\alpha}^{\beta_n}}{(\nu_{n+1}^{\beta_n+1} - \nu_n^{\beta_n+1})} \left(\frac{\nu}{\nu_{\alpha}} \right)^{\beta_n} \quad (\text{B3})$$

for $\nu_n \leq \nu \leq \nu_{n+1}$, with N_n the number of photons emitted between the n and $n+1$ resonances and β_n the spectral index [112]. The function above is normalized as $\int_{\nu_n}^{\nu_{n+1}} d\nu \varepsilon(\nu) = N_n$, with $\int_{\nu_{\alpha}}^{\nu_{LL}} d\nu \varepsilon(\nu) = \sum_n N_n \simeq 9690$ the total number of photons emitted between the Lyman- α and the Lyman limit. Although we keep this normalization as constant through our analysis, notice that changes in the number of photons which contribute to the Lyman- α flux could have a deep impact in the 21cm signal [136].

ACKNOWLEDGMENTS

LLH is supported by the FNRS, by the Strategic Research Program *High Energy Physics* and by the Research Council of the Vrije Universiteit Brussel. OM and PVD are supported by PROMETEO II/2014/050, by the Spanish MINECO Grants FPA2014-57816-P, FPA2017-85985-P and SEV-2014-0398 and by the European Union's Horizon 2020 research and innovation program under the Marie Skłodowska-Curie grant agreements No. 690575 and 674896.

-
- [1] C. Boehm, H. Mathis, J. Devriendt and J. Silk, *Non-linear evolution of suppressed dark matter primordial power spectra*, *Mon. Not. Roy. Astron. Soc.* **360** (2005) 282–287, [[astro-ph/0309652](#)].
 - [2] C. Boehm, J. A. Schewtschenko, R. J. Wilkinson, C. M. Baugh and S. Pascoli, *Using the Milky Way satellites to study interactions between cold dark matter and radiation*, *Mon. Not. Roy. Astron. Soc.* **445** (2014) L31–L35, [[1404.7012](#)].
 - [3] J. A. Schewtschenko, R. J. Wilkinson, C. M. Baugh, C. Boehm and S. Pascoli, *Dark matter-radiation interactions: the impact on dark matter haloes*, *Mon. Not. Roy. Astron. Soc.* **449** (2015) 3587–3596, [[1412.4905](#)].
 - [4] J. A. Schewtschenko et al., *Dark matter-radiation interactions: the structure of Milky Way satellite galaxies*, *Mon. Not. Roy. Astron. Soc.* **461** (2016) 2282–2287, [[1512.06774](#)].
 - [5] F.-Y. Cyr-Racine, R. de Putter, A. Raccanelli and K. Sigurdson, *Constraints on Large-Scale Dark Acoustic Oscillations from Cosmology*, *Phys. Rev.* **D89** (2014) 063517, [[1310.3278](#)].
 - [6] M. R. Buckley, J. Zavala, F.-Y. Cyr-Racine, K. Sigurdson and M. Vogelsberger, *Scattering, Damping, and Acoustic Oscillations: Simulating the Structure of Dark Matter Halos with Relativistic Force Carriers*, *Phys. Rev.* **D90** (2014) 043524, [[1405.2075](#)].
 - [7] M. Vogelsberger, J. Zavala, F.-Y. Cyr-Racine, C. Pfrommer, T. Bringmann and K. Sigurdson, *ETHOS – an effective theory of structure formation: dark matter physics as a possible explanation of the small-scale CDM problems*, *Mon. Not. Roy. Astron. Soc.* **460** (2016) 1399–1416, [[1512.05349](#)].
 - [8] F.-Y. Cyr-Racine et al., *ETHOS—an effective theory of structure formation: From dark particle physics to the matter distribution of the Universe*, *Phys. Rev.* **D93** (2016) 123527, [[1512.05344](#)].
 - [9] L. G. van den Aarssen, T. Bringmann and C. Pfrommer, *Is dark matter with long-range interactions a solution to all small-scale problems of Λ CDM cosmology?*, *Phys. Rev. Lett.* **109** (2012) 231301, [[1205.5809](#)].
 - [10] T. Bringmann, H. T. Ihle, J. Kersten and P. Walia, *Suppressing structure formation at dwarf galaxy scales and below: late kinetic decoupling as a compelling alternative to warm dark matter*, *Phys. Rev.* **D94** (2016) 103529, [[1603.04884](#)].
 - [11] C. Boehm, P. Fayet and R. Schaeffer, *Constraining dark matter candidates from structure formation*, *Phys. Lett.* **B518** (2001) 8–14, [[astro-ph/0012504](#)].
 - [12] C. Boehm, A. Riazuelo, S. H. Hansen and R. Schaeffer, *Interacting dark matter disguised as warm dark matter*, *Phys. Rev.* **D66** (2002) 083505, [[astro-ph/0112522](#)].
 - [13] C. Boehm and R. Schaeffer, *Constraints on dark matter interactions from structure formation: Damping lengths*, *Astron. Astrophys.* **438** (2005) 419–442, [[astro-ph/0410591](#)].
 - [14] R. Murgia, A. Merle, M. Viel, M. Totzauer and A. Schneider, *“Non-cold” dark matter at small scales: a general approach*, *JCAP* **1711** (2017) 046, [[1704.07838](#)].

- [15] J. S. Bullock and M. Boylan-Kolchin, *Small-Scale Challenges to the Λ CDM Paradigm*, *Ann. Rev. Astron. Astrophys.* **55** (2017) 343–387, [[1707.04256](#)].
- [16] M. Viel, G. D. Becker, J. S. Bolton and M. G. Haehnelt, *Warm dark matter as a solution to the small scale crisis: New constraints from high redshift Lyman-alpha forest data*, *Phys. Rev.* **D88** (2013) 043502, [[1306.2314](#)].
- [17] M. Viel, J. Lesgourgues, M. G. Haehnelt, S. Matarrese and A. Riotto, *Constraining warm dark matter candidates including sterile neutrinos and light gravitinos with WMAP and the Lyman-alpha forest*, *Phys. Rev.* **D71** (2005) 063534, [[astro-ph/0501562](#)].
- [18] U. Seljak, A. Makarov, P. McDonald and H. Trac, *Can sterile neutrinos be the dark matter?*, *Phys. Rev. Lett.* **97** (2006) 191303, [[astro-ph/0602430](#)].
- [19] M. Viel, J. Lesgourgues, M. G. Haehnelt, S. Matarrese and A. Riotto, *Can sterile neutrinos be ruled out as warm dark matter candidates?*, *Phys. Rev. Lett.* **97** (2006) 071301, [[astro-ph/0605706](#)].
- [20] G. Mangano, A. Melchiorri, P. Serra, A. Cooray and M. Kamionkowski, *Cosmological bounds on dark matter-neutrino interactions*, *Phys. Rev.* **D74** (2006) 043517, [[astro-ph/0606190](#)].
- [21] M. Viel et al., *How cold is cold dark matter? Small scales constraints from the flux power spectrum of the high-redshift Lyman-alpha forest*, *Phys. Rev. Lett.* **100** (2008) 041304, [[0709.0131](#)].
- [22] A. Boyarsky, J. Lesgourgues, O. Ruchayskiy and M. Viel, *Lyman-alpha constraints on warm and on warm-plus-cold dark matter models*, *JCAP* **0905** (2009) 012, [[0812.0010](#)].
- [23] P. Serra, F. Zalamea, A. Cooray, G. Mangano and A. Melchiorri, *Constraints on neutrino – dark matter interactions from cosmic microwave background and large scale structure data*, *Phys. Rev.* **D81** (2010) 043507, [[0911.4411](#)].
- [24] S. D. McDermott, H.-B. Yu and K. M. Zurek, *Turning off the Lights: How Dark is Dark Matter?*, *Phys. Rev.* **D83** (2011) 063509, [[1011.2907](#)].
- [25] R. J. Wilkinson, J. Lesgourgues and C. Boehm, *Using the CMB angular power spectrum to study Dark Matter-photon interactions*, *JCAP* **1404** (2014) 026, [[1309.7588](#)].
- [26] A. D. Dolgov, S. L. Dubovsky, G. I. Rubtsov and I. I. Tkachev, *Constraints on millicharged particles from Planck data*, *Phys. Rev.* **D88** (2013) 117701, [[1310.2376](#)].
- [27] R. J. Wilkinson, C. Boehm and J. Lesgourgues, *Constraining Dark Matter-Neutrino Interactions using the CMB and Large-Scale Structure*, *JCAP* **1405** (2014) 011, [[1401.7597](#)].
- [28] A. Schneider, *Structure formation with suppressed small-scale perturbations*, *Mon. Not. Roy. Astron. Soc.* **451** (2015) 3117–3130, [[1412.2133](#)].
- [29] M. Escudero, O. Mena, A. C. Vincent, R. J. Wilkinson and C. Boehm, *Exploring dark matter microphysics with galaxy surveys*, *JCAP* **1509** (2015) 034, [[1505.06735](#)].
- [30] Y. Ali-Haïmoud, J. Chluba and M. Kamionkowski, *Constraints on Dark Matter Interactions with Standard Model Particles from Cosmic Microwave Background Spectral Distortions*, *Phys. Rev. Lett.* **115** (2015) 071304, [[1506.04745](#)].
- [31] J. Baur, N. Palanque-Delabrouille, C. Yèche, C. Magneville and M. Viel, *Lyman-alpha Forests cool Warm Dark Matter*, *JCAP* **1608** (2016) 012, [[1512.01981](#)].
- [32] R. Diamanti, S. Ando, S. Gariazzo, O. Mena and C. Weniger, *Cold dark matter plus not-so-clumpy dark relics*, *JCAP* **1706** (2017) 008, [[1701.03128](#)].
- [33] V. Irsic et al., *New Constraints on the free-streaming of warm dark matter from intermediate and small scale Lyman-alpha forest data*, *Phys. Rev.* **D96** (2017) 023522, [[1702.01764](#)].
- [34] C. Yèche, N. Palanque-Delabrouille, J. Baur and H. du Mas des Bourboux, *Constraints on neutrino masses from Lyman-alpha forest power spectrum with BOSS and XQ-100*, *JCAP* **1706** (2017) 047, [[1702.03314](#)].
- [35] S. Gariazzo, M. Escudero, R. Diamanti and O. Mena, *Cosmological searches for a noncold dark matter component*, *Phys. Rev.* **D96** (2017) 043501, [[1704.02991](#)].
- [36] J. A. D. Diacoumis and Y. Y. Y. Wong, *Using CMB spectral distortions to distinguish between dark matter solutions to the small-scale crisis*, *JCAP* **1709** (2017) 011, [[1707.07050](#)].
- [37] E. Di Valentino, C. Boehm, E. Hivon and F. R. Bouchet, *Reducing the H_0 and σ_8 tensions with Dark Matter-neutrino interactions*, *Phys. Rev.* **D97** (2018) 043513, [[1710.02559](#)].
- [38] A. O.-D. Campo, C. Boehm, S. Palomares-Ruiz and S. Pascoli, *Dark matter-neutrino interactions through the lens of their cosmological implications*, *Phys. Rev. D* **97** **075939** (2018) , [[1711.05283](#)].
- [39] J. Stadler and C. Boehm, *CMB constraints on γ -CDM interactions revisited*, **1802.06589**.
- [40] A. D. Rivero, C. Dvorkin, F.-Y. Cyr-Racine, J. Zavala and M. Vogelsberger, *Gravitational Lensing and the Power Spectrum of Dark Matter Substructure: Insights from the ETHOS N-body Simulations*, **1809.00004**.
- [41] M. R. Lovell et al., *ETHOS – an effective theory of structure formation: Predictions for the high-redshift Universe – abundance of galaxies and reionization*, *Mon. Not. Roy. Astron. Soc.* **477** (2018) 2526–2539, [[1711.10497](#)].
- [42] P. Dayal, A. Mesinger and F. Pacucci, *Early galaxy formation in warm dark matter cosmologies*, *Astrophys. J.* **806** (2015) 67, [[1408.1102](#)].
- [43] S. Bose, C. S. Frenk, J. Hou, C. G. Lacey and M. R. Lovell, *Reionization in sterile neutrino cosmologies*, *Mon. Not. Roy. Astron. Soc.* **463** (2016) 3848–3859, [[1605.03179](#)].
- [44] L. Lopez-Honorez, O. Mena, S. Palomares-Ruiz and P. Villanueva-Domingo, *Warm dark matter and the ionization history of the Universe*, *Phys. Rev.* **D96** (2017) 103539, [[1703.02302](#)].
- [45] R. Barkana, Z. Haiman and J. P. Ostriker, *Constraints on warm dark matter from cosmological reionization*, *Astrophys. J.* **558** (2001) 482, [[astro-ph/0102304](#)].
- [46] N. Yoshida, A. Sokasian, L. Hernquist and V. Springel, *Early structure formation and reionization in a warm dark matter cosmology*, *Astrophys. J.* **591** (2003) L1–L4, [[astro-ph/0303622](#)].
- [47] R. S. Somerville, J. S. Bullock and M. Livio, *The epoch of reionization in models with reduced small scale power*, *Astrophys. J.* **593** (2003) 616–621,

- [astro-ph/0303481].
- [48] B. Yue and X. Chen, *Reionization in the Warm Dark Matter Model*, *Astrophys. J.* **747** (2012) 127, [1201.3686].
- [49] F. Pacucci, A. Mesinger and Z. Haiman, *Focusing on Warm Dark Matter with Lensed High-redshift Galaxies*, *Mon. Not. Roy. Astron. Soc.* **435** (2013) L53, [1306.0009].
- [50] A. Mesinger, A. Ewall-Wice and J. Hewitt, *Reionization and beyond: detecting the peaks of the 21 cm signal*, *Mon. Not. Roy. Astron. Soc.* **439** (2014) 3262–3274, [1310.0465].
- [51] C. Schultz, J. Oñorbe, K. N. Abazajian and J. S. Bullock, *The High- z Universe Confronts Warm Dark Matter: Galaxy Counts, Reionization and the Nature of Dark Matter*, *Mon. Not. Roy. Astron. Soc.* **442** (2014) 1597–1609, [1401.3769].
- [52] A. Lapi and L. Danese, *Cold or Warm? Constraining Dark Matter with Primeval Galaxies and Cosmic Reionization after Planck*, *JCAP* **1509** (2015) 003, [1508.02147].
- [53] S. Bose et al., *Substructure and galaxy formation in the Copernicus Complexio warm dark matter simulations*, *Mon. Not. Roy. Astron. Soc.* **464** (2017) 4520–4533, [1604.07409].
- [54] P. S. Corasaniti, S. Agarwal, D. J. E. Marsh and S. Das, *Constraints on dark matter scenarios from measurements of the galaxy luminosity function at high redshifts*, *Phys. Rev.* **D95** (2017) 083512, [1611.05892].
- [55] N. Menci, A. Grazian, M. Castellano and N. G. Sanchez, *A Stringent Limit on the Warm Dark Matter Particle Masses from the Abundance of $z=6$ Galaxies in the Hubble Frontier Fields*, *Astrophys. J.* **825** (2016) L1, [1606.02530].
- [56] P. Villanueva-Domingo, N. Y. Gnedin and O. Mena, *Warm Dark Matter and Cosmic Reionization*, *Astrophys. J.* **852** (2018) 139, [1708.08277].
- [57] S. Das, R. Mondal, V. Rentala and S. Suresh, *On dark matter - dark radiation interaction and cosmic reionization*, *JCAP* **1808** (2018) 045, [1712.03976].
- [58] M. Escudero, L. Lopez-Honorez, O. Mena, S. Palomares-Ruiz and P. Villanueva-Domingo, *A fresh look into the interacting dark matter scenario*, *JCAP* **1806** (2018) 007, [1803.08427].
- [59] M. Sitwell, A. Mesinger, Y.-Z. Ma and K. Sigurdson, *The Imprint of Warm Dark Matter on the Cosmological 21-cm Signal*, *Mon. Not. Roy. Astron. Soc.* **438** (2014) 2664–2671, [1310.0029].
- [60] I. P. Carucci, F. Villaescusa-Navarro, M. Viel and A. Lapi, *Warm dark matter signatures on the 21cm power spectrum: Intensity mapping forecasts for SKA*, *JCAP* **1507** (2015) 047, [1502.06961].
- [61] J. D. Bowman, A. E. E. Rogers, R. A. Monsalve, T. J. Mozdzen and N. Mahesh, *An absorption profile centred at 78 megahertz in the sky-averaged spectrum*, *Nature* **555** (2018) 67–70.
- [62] R. Hills, G. Kulkarni, P. D. Meerburg and E. Puchwein, *Concerns about Modelling of Foregrounds and the 21-cm Signal in EDGES data*, **1805.01421**.
- [63] R. F. Bradley, K. Tauscher, D. Rapetti and J. O. Burns, *A Ground Plane Artifact that Induces an Absorption Profile in Averaged Spectra from Global 21-cm Measurements - with Possible Application to EDGES*, **1810.09015**.
- [64] A. Berlin, D. Hooper, G. Krnjaic and S. D. McDermott, *Severely Constraining Dark Matter Interpretations of the 21-cm Anomaly*, *Phys. Rev. Lett.* **121** (2018) 011102, [1803.02804].
- [65] G. D’Amico, P. Panci and A. Strumia, *Bounds on Dark Matter annihilations from 21 cm data*, *Phys. Rev. Lett.* **121** (2018) 011103, [1803.03629].
- [66] H. Liu and T. R. Slatyer, *Implications of a 21-cm signal for dark matter annihilation and decay*, *Phys. Rev.* **D98** (2018) 023501, [1803.09739].
- [67] A. Mitridate and A. Podo, *Bounds on Dark Matter decay from 21 cm line*, *JCAP* **1805** (2018) 069, [1803.11169].
- [68] M. Valdés, C. Evoli, A. Mesinger, A. Ferrara and N. Yoshida, *The nature of dark matter from the global high redshift HI 21 cm signal*, *Mon. Not. Roy. Astron. Soc.* **429** (2013) 1705–1716, [1209.2120].
- [69] C. Evoli, A. Mesinger and A. Ferrara, *Unveiling the nature of dark matter with high redshift 21 cm line experiments*, *JCAP* **1411** (2014) 024, [1408.1109].
- [70] L. Lopez-Honorez, O. Mena, A. Moliné, S. Palomares-Ruiz and A. C. Vincent, *The 21 cm signal and the interplay between dark matter annihilations and astrophysical processes*, *JCAP* **1608** (2016) 004, [1603.06795].
- [71] M. Pospelov, J. Pradler, J. T. Ruderman and A. Urbano, *Room for New Physics in the Rayleigh-Jeans Tail of the Cosmic Microwave Background*, *Phys. Rev. Lett.* **121** (2018) 031103, [1803.07048].
- [72] D. Aristizabal Sierra and C. S. Fong, *The EDGES signal: An imprint from the mirror world?*, *Phys. Lett.* **B784** (2018) 130–136, [1805.02685].
- [73] K. K. Boddy, V. Gluscevic, V. Poulin, E. D. Kovetz, M. Kamionkowski and R. Barkana, *A Critical Assessment of CMB Limits on Dark Matter-Baryon Scattering: New Treatment of the Relative Bulk Velocity*, **1808.00001**.
- [74] E. D. Kovetz, V. Poulin, V. Gluscevic, K. K. Boddy, R. Barkana and M. Kamionkowski, *Tighter Limits on Dark Matter Explanations of the Anomalous EDGES 21cm Signal*, **1807.11482**.
- [75] R. Barkana, N. J. Outmezguine, D. Redigolo and T. Volansky, *Signs of Dark Matter at 21-cm?*, **1803.03091**.
- [76] R. Barkana, *Possible interaction between baryons and dark-matter particles revealed by the first stars*, *Nature* **555** (2018) 71–74, [1803.06698].
- [77] A. Schneider, *Constraining Non-Cold Dark Matter Models with the Global 21-cm Signal*, *Phys. Rev.* **D98** (2018) 063021, [1805.00021].
- [78] M. Safarzadeh, E. Scannapieco and A. Babul, *A limit on the warm dark matter particle mass from the redshifted 21 cm absorption line*, *Astrophys. J.* **859** (2018) L18, [1803.08039].
- [79] A. Lidz and L. Hui, *The Implications of a Pre-reionization 21 cm Absorption Signal for Fuzzy Dark Matter*, *Phys. Rev.* **D98** (2018) 023011, [1805.01253].
- [80] Á. Moliné, J. A. Schewtschenko, S. Palomares-Ruiz, C. Boehm and C. M. Baugh, *Isotropic extragalactic flux from dark matter annihilations: lessons from interacting dark matter scenarios*, *JCAP* **1608** (2016)

- 069, [1602.07282].
- [81] J. A. Schewtschenko, *Cosmological Simulations with Dark Matter from beyond the Standard Model*. PhD thesis, Durham U., 2016.
 - [82] C. Dvorkin, K. Blum and M. Kamionkowski, *Constraining Dark Matter-Baryon Scattering with Linear Cosmology*, *Phys. Rev.* **D89** (2014) 023519, [1311.2937].
 - [83] N. Vinyoles and H. Vogel, *Minicharged Particles from the Sun: A Cutting-Edge Bound*, *JCAP* **1603** (2016) 002, [1511.01122].
 - [84] P. Bode, J. P. Ostriker and N. Turok, *Halo formation in warm dark matter models*, *Astrophys. J.* **556** (2001) 93–107, [astro-ph/0010389].
 - [85] A. Knebe, J. E. G. Devriendt, A. Mahmood and J. Silk, *Merger histories in WDM structure formation scenarios*, *Mon. Not. Roy. Astron. Soc.* **329** (2002) 813, [astro-ph/0105316].
 - [86] P. Colin, O. Valenzuela and V. Avila-Reese, *On the Structure of Dark Matter Halos at the Damping Scale of the Power Spectrum with and without Relict Velocities*, *Astrophys. J.* **673** (2008) 203–214, [0709.4027].
 - [87] J. Zavala et al., *The velocity function in the local environment from LCDM and LWDM constrained simulations*, *Astrophys. J.* **700** (2009) 1779–1793, [0906.0585].
 - [88] R. E. Smith and K. Markovic, *Testing the Warm Dark Matter paradigm with large-scale structures*, *Phys. Rev.* **D84** (2011) 063507, [1103.2134].
 - [89] M. R. Lovell et al., *The Haloes of Bright Satellite Galaxies in a Warm Dark Matter Universe*, *Mon. Not. Roy. Astron. Soc.* **420** (2012) 2318–2324, [1104.2929].
 - [90] A. Schneider, R. E. Smith, A. V. Macciò and B. Moore, *Nonlinear Evolution of Cosmological Structures in Warm Dark Matter Models*, *Mon. Not. Roy. Astron. Soc.* **424** (2012) 684, [1112.0330].
 - [91] E. Polisensky and M. Ricotti, *Massive Milky Way Satellites in Cold and Warm Dark Matter: Dependence on Cosmology*, *Mon. Not. Roy. Astron. Soc.* **437** (2014) 2922–2931, [1310.0430].
 - [92] M. R. Lovell et al., *The properties of warm dark matter haloes*, *Mon. Not. Roy. Astron. Soc.* **439** (2014) 300–317, [1308.1399].
 - [93] R. Kennedy, C. Frenk, S. Cole and A. Benson, *Constraining the warm dark matter particle mass with Milky Way satellites*, *Mon. Not. Roy. Astron. Soc.* **442** (2014) 2487–2495, [1310.7739].
 - [94] C. Destri, H. J. de Vega and N. G. Sánchez, *Warm dark matter primordial spectra and the onset of structure formation at redshift z* , *Phys. Rev.* **D88** (2013) 083512, [1308.1109].
 - [95] R. E. Angulo, O. Hahn and T. Abel, *The Warm DM halo mass function below the cut-off scale*, *Mon. Not. Roy. Astron. Soc.* **434** (2013) 3337, [1304.2406].
 - [96] A. J. Benson et al., *Dark Matter Halo Merger Histories Beyond Cold Dark Matter: I - Methods and Application to Warm Dark Matter*, *Mon. Not. Roy. Astron. Soc.* **428** (2013) 1774, [1209.3018].
 - [97] A. Kamada, N. Yoshida, K. Kohri and T. Takahashi, *Structure of Dark Matter Halos in Warm Dark Matter models and in models with Long-Lived Charged Massive Particles*, *JCAP* **1303** (2013) 008, [1301.2744].
 - [98] M. R. Lovell et al., *Satellite galaxies in semi-analytic models of galaxy formation with sterile neutrino dark matter*, *Mon. Not. Roy. Astron. Soc.* **461** (2016) 60–72, [1511.04078].
 - [99] A. D. Ludlow et al., *The Mass-Concentration-Redshift Relation of Cold and Warm Dark Matter Halos*, *Mon. Not. Roy. Astron. Soc.* **460** (2016) 1214–1232, [1601.02624].
 - [100] L. Wang et al., *The galaxy population in cold and warm dark matter cosmologies*, *Mon. Not. Roy. Astron. Soc.* **468** (2017) 4579–4591, [1612.04540].
 - [101] M. R. Lovell et al., *Addressing the too big to fail problem with baryon physics and sterile neutrino dark matter*, *Mon. Not. Roy. Astron. Soc.* **468** (2017) 2836–2849, [1611.00005].
 - [102] T. Nakama, J. Chluba and M. Kamionkowski, *Shedding light on the small-scale crisis with CMB spectral distortions*, *Phys. Rev.* **D95** (2017) 121302, [1703.10559].
 - [103] P. Madau, A. Meiksin and M. J. Rees, *21-CM tomography of the intergalactic medium at high redshift*, *Astrophys. J.* **475** (1997) 429, [astro-ph/9608010].
 - [104] S. Furlanetto, S. P. Oh and F. Briggs, *Cosmology at Low Frequencies: The 21 cm Transition and the High-Redshift Universe*, *Phys. Rept.* **433** (2006) 181–301, [astro-ph/0608032].
 - [105] J. R. Pritchard and A. Loeb, *21-cm cosmology*, *Rept. Prog. Phys.* **75** (2012) 086901, [1109.6012].
 - [106] S. R. Furlanetto, *The 21-cm Line as a Probe of Reionization*, in *Understanding the Epoch of Cosmic Reionization: Challenges and Progress* (A. Mesinger, ed.), vol. 423, pp. 247–280. Springer International Publishing, 2016. 1511.01131.
 - [107] C. M. Hirata, *Wouthuysen-Field coupling strength and application to high-redshift 21 cm radiation*, *Mon. Not. Roy. Astron. Soc.* **367** (2006) 259–274, [astro-ph/0507102].
 - [108] S. A. Wouthuysen, *On the excitation mechanism of the 21-cm (radio-frequency) interstellar hydrogen emission line.*, *Astrophys. J.* **57** (1952) 31–32.
 - [109] G. B. Field, *Excitation of the Hydrogen 21-CM Line*, *Proceedings of the IRE* **46** (Jan., 1958) 240–250.
 - [110] X.-L. Chen and J. Miralda-Escude, *The spin - kinetic temperature coupling and the heating rate due to Lyman - alpha scattering before reionization: Predictions for 21cm emission and absorption*, *Astrophys. J.* **602** (2004) 1–11, [astro-ph/0303395].
 - [111] A. Mesinger, S. Furlanetto and R. Cen, *21cmFAST: A Fast, Semi-Numerical Simulation of the High-Redshift 21-cm Signal*, *Mon. Not. Roy. Astron. Soc.* **411** (2011) 955, [1003.3878].
 - [112] R. Barkana and A. Loeb, *Detecting the earliest galaxies through two new sources of 21cm fluctuations*, *Astrophys. J.* **626** (2005) 1–11, [astro-ph/0410129].
 - [113] R. S. de Souza et al., *Constraints on Warm Dark Matter models from high-redshift long gamma-ray bursts*, *Mon. Not. Roy. Astron. Soc.* **432** (2013) 3218, [1303.5060].
 - [114] Á. Moliné, M. A. Sánchez-Conde, S. Palomares-Ruiz and F. Prada, *Characterization of subhalo structural properties and implications for dark matter annihilation signals*, *Mon. Not. Roy. Astron. Soc.* **466** (2017) 4974–4990, [1603.04057].

- [115] R. Barkana and A. Loeb, *In the beginning: The First sources of light and the reionization of the Universe*, *Phys. Rept.* **349** (2001) 125–238, [[astro-ph/0010468](#)].
- [116] A. E. Evrard, *Formation and evolution of X-ray clusters - A hydrodynamic simulation of the intracuster medium*, *Astrophys. J.* **363** (1990) 349–366.
- [117] A. Blanchard, D. Vall-Gabaud and G. A. Mamon, *The origin of the galaxy luminosity function and the thermal evolution of the intergalactic medium*, *Astron. Astrophys.* **264** (1992) 365–378.
- [118] M. Tegmark et al., *How small were the first cosmological objects?*, *Astrophys. J.* **474** (1997) 1–12, [[astro-ph/9603007](#)].
- [119] Z. Haiman, T. Abel and M. J. Rees, *The radiative feedback of the first cosmological objects*, *Astrophys. J.* **534** (2000) 11–24, [[astro-ph/9903336](#)].
- [120] B. Ciardi, A. Ferrara, F. Governato and A. Jenkins, *Inhomogeneous reionization regulated by radiative and stellar feedbacks*, *Mon. Not. Roy. Astron. Soc.* **314** (2000) 611, [[astro-ph/9907189](#)].
- [121] J. H. Wise and T. Abel, *Suppression of H_2 Cooling in the Ultraviolet Background*, *Astrophys. J.* **671** (2007) 1559, [[0707.2059](#)].
- [122] J. H. Wise, V. G. Demchenko, M. T. Halicek, M. L. Norman, M. J. Turk, T. Abel et al., *The birth of a galaxy – III. Propelling reionization with the faintest galaxies*, *Mon. Not. Roy. Astron. Soc.* **442** (2014) 2560–2579, [[1403.6123](#)].
- [123] H. Xu, J. H. Wise, M. L. Norman, K. Ahn and B. W. O’Shea, *Galaxy Properties and UV Escape Fractions during the Epoch of Reionization: Results from the Renaissance Simulations*, *Astrophys. J.* **833** (Dec., 2016) 84, [[1604.07842](#)].
- [124] X. Ma, P. F. Hopkins, S. Garrison-Kimmel, C.-A. Faucher-Giguère, E. Quataert, M. Boylan-Kolchin et al., *Simulating galaxies in the reionization era with FIRE-2: galaxy scaling relations, stellar mass functions, and luminosity functions*, **1706.06605**.
- [125] J. Rosdahl, H. Katz, J. Blaizot, T. Kimm, L. Michel-Dansac, T. Garel et al., *The SPHINX cosmological simulations of the first billion years: the impact of binary stars on reionization*, *mnras* **479** (Sept., 2018) 994–1016, [[1801.07259](#)].
- [126] N. Mashian, P. A. Oesch and A. Loeb, *An empirical model for the galaxy luminosity and star formation rate function at high redshift*, *mnras* **455** (Jan., 2016) 2101–2109, [[1507.00999](#)].
- [127] N. Leite, C. Evoli, M. D’Angelo, B. Ciardi, G. Sigl and A. Ferrara, *Do Cosmic Rays Heat the Early Intergalactic Medium?*, *Mon. Not. Roy. Astron. Soc.* **469** (2017) 416–424, [[1703.09337](#)].
- [128] B. Greig and A. Mesinger, *21CMMC: an MCMC analysis tool enabling astrophysical parameter studies of the cosmic 21 cm signal*, *Mon. Not. Roy. Astron. Soc.* **449** (2015) 4246–4263, [[1501.06576](#)].
- [129] S. Mineo, M. Gilfanov and R. Sunyaev, *X-ray emission from star-forming galaxies - II. Hot interstellar medium*, *Mon. Not. Roy. Astron. Soc.* **426** (2012) 1870, [[1205.3715](#)].
- [130] R. A. Monsalve, B. Greig, J. D. Bowman, A. Mesinger, A. E. E. Rogers, T. J. Mozdzen et al., *Results from EDGES High-Band: II. Constraints on Parameters of Early Galaxies*, *Astrophys. J.* **863** (2018) 11, [[1806.07774](#)].
- [131] W. H. Press and P. Schechter, *Formation of galaxies and clusters of galaxies by selfsimilar gravitational condensation*, *Astrophys. J.* **187** (1974) 425–438.
- [132] R. K. Sheth and G. Tormen, *Large scale bias and the peak background split*, *Mon. Not. Roy. Astron. Soc.* **308** (1999) 119, [[astro-ph/9901122](#)].
- [133] R. K. Sheth, H. J. Mo and G. Tormen, *Ellipsoidal collapse and an improved model for the number and spatial distribution of dark matter haloes*, *Mon. Not. Roy. Astron. Soc.* **323** (2001) 1, [[astro-ph/9907024](#)].
- [134] R. K. Sheth and G. Tormen, *An Excursion set model of hierarchical clustering : Ellipsoidal collapse and the moving barrier*, *Mon. Not. Roy. Astron. Soc.* **329** (2002) 61, [[astro-ph/0105113](#)].
- [135] J. R. Pritchard and S. R. Furlanetto, *Descending from on high: lyman series cascades and spin-kinetic temperature coupling in the 21 cm line*, *Mon. Not. Roy. Astron. Soc.* **367** (2006) 1057–1066, [[astro-ph/0508381](#)].
- [136] S. Witte, P. Villanueva-Domingo, S. Gariazzo, O. Mena and S. Palomares-Ruiz, *EDGES result versus CMB and low-redshift constraints on ionization histories*, *Phys. Rev.* **D97** (2018) 103533, [[1804.03888](#)].